On the Spatial and Temporal Variations of Primary Production in the South China Sea

Luping Song, Zhongping Lee, *Member, IEEE*, Shaoling Shang, Bangqin Huang, Jinghui Wu, Zelun Wu, Wenfang Lu, and Xin Liu

***Abstract*— Primary production (PP) of the South China Sea (SCS) basin area (waters depth deeper than 200 m) is estimated using satellite products, with an overarching goal to reliably characterize the spatial distribution and temporal variation of PP of this important marginal sea. Among the PP models used, the absorption-based model (AbPM) showed better performance ($R^2 = 0.47$ and $N = 39$). In comparison, the R^2 value is 0.26 for a chlorophyll-based model [vertically generalized production model (VGPM)] and 0.15 for the carbon-based model (CbPM). Furthermore, we observed that the PP spatial patterns obtained from these models were similar but disagree on the annual PP magnitude, where VGPM and CbPM, respectively, obtained ∼50% lower and ∼40% higher annual PP compared to that obtained by AbPM. In particular, after analysis using empirical orthogonal functions (EOFs), the upwelling-induced high PP off Luzon (winter) and Vietnam coast (summer) was clearly reflected in the first EOF mode of the AbPM results, and its principal component 1 has shown a decreasing trend for the period of 2003–2019 (−15.0% yr^{-1} for winter, $p < 0.05$; −14.7% yr^{-1} for summer, $p < 0.05$), which reflects the impact of weakening wind and higher sea surface temperature in the SCS. For the results of VGPM and CbPM, however, no strong relationships were found with the main regional oceanographic features. These results suggested that the spatiotemporal variations of SCS PP obtained from AbPM are more reasonable and further highlight the importance of a robust model in reliably capturing large-scale spatiotemporal dynamics of PP in marine environments.**

***Index Terms*— Model, primary production (PP), remote sensing, South China Sea (SCS), spatiotemporal variability.**

I. Introduction

PRIMARY production (PP) represents the capacity of marine phytoplankton to fix carbon dioxide (CO_2), accounting for about half of global biological carbon fixation [4]. It transfers atmospheric carbon into the ocean interior through the "biological pump" [5], a process that reduces atmospheric CO_2 by about 180 ppm compared to an ocean without biological pump [6] and helps to slow global warming. In this regard, PP is an important indicator for assessing the contributions of marine ecosystems to long-term climate change [7], [8]. The South China Sea (SCS), situated in the western side of the Pacific Ocean, is an important region for the study of the Pacific and global climate and phytoplankton interactions [9], [10], which also exchanges carbon with "the engine of global climate" (the western Pacific warm pool) through the Luzon Strait. It has been suggested that PP in the SCS is about 545.1 Tg C·yr^{-1} (10^{12} g·C), contributing ∼64% of PP in China Seas [9], [10], [11]. However, due to the difficulties in measuring PP in situ, compared to other major biological factors, there has been much less PP data in SCS to adequately characterize its spatial distribution and temporal variation [12]. As a consequence, the response of PP in SCS in the context of climate change is far from clear.

In the past two decades, based on in situ measurements of PP in the SCS, Ning et al. [9] provided an initial description of the spatial and temporal variations of PP in SCS. Due to limited coverage from these measurements, it is necessary to compile long-term PP data of such large areas based on satellite observations [13]. For this purpose, many models have since been developed to convert satellite products to PP [14], [15], [16], [17]. The vertically generalized production model (VGPM) [16] has been one of the most applied models to estimate PP from satellite ocean color remote sensing and the scheme to study PP in the SCS [18], [19], [20], [21].

For instance, Tan and Shi [22] analyzed the spatial and temporal variation of PP in SCS for the period of 1998–2006 using a modified VGPM and found that the PP maximum occurred mainly in the northwestern part of the Luzon Strait on winter and in eastern Vietnam on summer, with low PP in the basin. This conclusion was echoed by Kong et al. [20] who reported the spatial distribution of PP for the period of 1998–2016 based on spatial distribution characteristics obtained by VGPM. Generally, these findings are consistent with the results observed from field measurements [9]. On the temporal variations, Li et al. [23] applied VGPM to estimate PP in SCS and found no significant PP trend in the SCS between 1998 and 2002. Similar results were also found by Tan and Shi [22] after expanding the time range to 2006 along with a modified VGPM. Further extending the time scale and also based on VGPM, Kong et al. [20], however, found that the PP of the whole SCS was increasing at a rate of

Manuscript received 21 October 2022; revised 16 January 2023; accepted 28 January 2023. Date of publication 31 January 2023; date of current version 13 February 2023. This work was supported in part by the National Natural Science Foundation of China under Grant #41830102, Grant #42250710150, Grant #41941008, and Grant #41890803. *(Corresponding author: Zhongping Lee.)*

Luping Song, Zhongping Lee, Shaoling Shang, and Zelun Wu are with the State Key Laboratory of Marine Environmental Science, College of Ocean and Earth Sciences, Xiamen University, Xiamen 361102, China (e-mail: songluping1994@xmu.edu.cn; Zhongping.Lee@umb.edu; slshang@xmu.edu.cn; zelunwu@udel.edu).

Bangqin Huang and Xin Liu are with the State Key Laboratory of Marine Environmental Science, College of the Environment and Ecology, Xiamen University, Xiamen 361102, China (e-mail: bqhuang@xmu.edu.cn; liuxin1983@xmu.edu.cn).

Jinghui Wu is with the Lamont Doherty Earth Observatory, Columbia University, New York, NY 10027 USA (e-mail: jinghuiw@ldeo.columbia.edu).

Wenfang Lu is with the School of Marine Sciences, Sun Yat-sen University, Guangzhou 510275, China, and also with the Southern Marine Science and Engineering Guangdong Laboratory (Zhuhai), Zhuhai 519000, China (e-mail: luwf6@mail.sysu.edu.cn).

Digital Object Identifier 10.1109/TGRS.2023.3241209

2.95 mg·C·m^{-2} month^{-1} between 1998 and 2016. However, as pointed out in many studies [24], [25], [26], [27], there are large uncertainties in the VGPM-estimated PP, thus not clear how much the VGPM-estimated PP for waters in the SCS contains bias, consequently negatively affecting the analysis of its spatial distributions and long-term trends.

For VGPM, there are two primary sources of uncertainties in the estimation of PP, where the determination of the maximum carbon fixation rate within the water column ($P^B_{\rm opt}$) is the key and there are no feasible means yet for its accurate estimate from remote sensing [28]. Therefore, a model of estimating PP based on phytoplankton carbon ($C_{\rm ph}$, mg·m^{-3}) (termed as carbon-based model (CbPM) [28], [29]) has been developed, where the ratio of chlorophyll concentration (Chl, mg·m^{-3}) to $C_{\rm ph}$ is used to track changes in phytoplankton physiology [28], [29]. Separately, in view of the large uncertainties in estimating Chl from ocean color remote sensing, an absorption-based model (AbPM) was developed in a concept to bypass the estimation of Chl [30], [31]. Various studies [31], [32], [33] have suggested that at least the AbPM performed significantly better than VGPM on the remote estimation of PP due to its no involvement of the chlorophyll-specific absorption coefficient, which is a property varies widely and at present could not be accurately estimated remotely. It is thus important and useful to evaluate the PP spatial distribution and temporal variation in the SCS in the past decades using PP estimates from these different approaches. We therefore first used in situ PP from regions covering the northern SCS (NSCS), central SCS (CSCS), and western SCS (WSCS) for the period of 2009–2020 to evaluate the estimated PP from the three models. Furthermore, a long-term dataset of PP was constructed from satellite measurements for the period of 2003–2019. The goals of this study are thus twofold: 1) to identify a better strategy or model for the estimation of PP in SCS and 2) to obtain more reasonable spatial and temporal variations of PP in SCS from the long-term satellite ocean color measurements.

II. Data and Methods

A. Models for Primary Production Estimation

As mentioned above, three models, namely, VGPM, CbPM, and AbPM, which represent three different strategies for the estimation of PP, are evaluated in this study. VGPM is calculated as follows:

$$\mathrm{PP}_{\rm VGPM} = 0.66125 \times P^B_{\rm opt} \times \frac{\mathrm{PAR}(0)}{\mathrm{PAR}(0)+4.1} \times \mathrm{Z}_{\rm eu} \times \mathrm{Chl} \times \mathrm{DL} \tag{1}$$

with $\mathrm{PP}_{\rm VGPM}$ (mg·C·m^{-2}·d^{-1}) for total PP within the euphotic zone. Here, Chl is a proxy of phytoplankton biomass, $P^B_{\rm opt}$ (mg C (mg Chl) $^{-1}$·h^{-1}) is the maximum carbon fixation rate within the water column, which is modeled empirically as a seventh-order polynomial function of sea surface temperature (SST) (°C), and PAR(0) (mol photons m^{-2} d^{-1}) refers to daily photosynthetically available radiation at the surface, with DL (h) as the daily light hours. $Z_{\rm eu}$ (m) is the euphotic-zone depth defined here as the depth of 1% surface photosynthetically active radiation (PAR) in VGPM. Chl, SST, and PAR(0) are standard products from satellite ocean color missions, while $Z_{\rm eu}$ was estimated from Chl [34].

CbPM at depth z is expressed as [28]

$$\mathrm{PP}_{\rm CbPM} = C_{\rm ph}\left\{\left(b_{\rm bp}(440)\right\} \times \mu\left\{\mu_{\max}, \mathrm{Chl}{:}C_{\rm ph}, I_g\right\}\mathrm{PP}_{\rm CbPM}\right. \tag{2}$$

$$C_{\rm ph} = 13000 \times \left(b_{\rm bp}(440) - 0.00035\right) \tag{3}$$

where $\mu_{\max}$ is the maximum carbon-specific growth rate and taken as 2 day^{-1}. $C_{\rm ph}$ is calculated from particulate backscattering coefficients at 440 nm ($b_{\rm bp}(440)$, m^{-1}), which can be derived from remote sensing reflectance ($R_{\rm rs}$, sr^{-1}). Furthermore, phytoplankton growth rate is estimated from Chl:$C_{\rm ph}$ ratio and growth irradiance (I_g, mol photons m^{-2}·h^{-1}).

AbPM estimates PP at depth z as

$$\mathrm{PP}(z) = \int_{400}^{700} \phi(z) \times a_{\rm ph}(\lambda) \times E(z,\lambda) d\lambda \tag{4}$$

$$E(z,\lambda) = \mathrm{PAR}(0) \times \bar{E}_S(\lambda) \times \exp(-K_d(\lambda) \times z) \tag{5}$$

where ϕ is the quantum yield of phytoplankton photosynthesis, which varies with light intensity, and was modeled following Kiefer and Mitchell [35] after considering photoinhibition:

$$\phi = \phi_m \times K_\phi / \left(K_\phi + \mathrm{PAR}(z)\right) \times \exp(-\nu \times \mathrm{PAR}(z) \tag{6}$$

with K_ϕ the light intensity when ϕ is at half $\phi_{\rm m}$. The default values of $\phi_{\rm m}$ and K_ϕ for global applications are commonly taken as 0.06 mol·C·mol·photons^{-1} [36] and 10-mol·photons·m^{-2}·d^{-1} [35], respectively. ν is photoinhibition factor [37], with an average value of 0.01 (Ein·m^{-2}·d^{-1})$^{-1}$. $a_{\rm ph}$ is the absorption coefficient of phytoplankton and K_d is the diffuse attenuation coefficient of downwelling irradiance, and both can be derived from $R_{\rm rs}$ [38]. $\bar{E}_S$ is a normalized spectrum for downwelling solar radiation, which reflects the spectral shape of PAR at sea surface [38]. Finally, integrating PP(z) in the euphotic zone provides water-column primary production from AbPM ($\mathrm{PP}_{\rm AbPM}$). More detailed descriptions of AbPM for PP can be found in Zoffoli et al. [38].

B. Modeled PP Using Satellite and in Situ Inputs

For model validations and analyses of long-term trend, eight-day composite and monthly mean PP products from VGPM and CbPM estimated using data from the Moderate Resolution Imaging Spectroradiometer-Aqua (Aqua-MODIS) for the period of January 2003–December 2019 were downloaded from the Oregon Ocean Productivity Laboratory (OSU: http://sites.science.oregonstate.edu/ocean.productivity/index.php). The spatial resolution of these data products is 9 km.

There are no standard PP products from AbPM yet for download, and therefore, PP of AbPM was estimated based on standard satellite data [$R_{\rm rs}$ and PAR(0)] downloaded from NASA (https://oceancolor.gsfc.nasa.gov). Specifically, Aqua-MODIS eight-day composite and monthly mean Level-3 $R_{\rm rs}$ (data processing version R2014.0) products, also at 9-km resolution, were downloaded and fed to the quasi-analytical algorithm (QAA, Version 6, http://www.

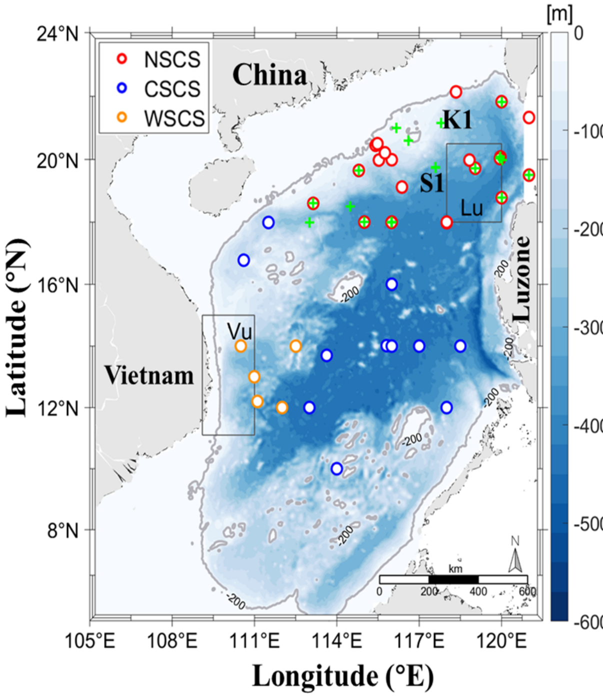

Fig. 1. Locations of field measurements and two well-known upwelling zones in the SCS. The solid gray line represents 200-m water depth. Red dots: NSCS dataset; blue dots: CSCS dataset; yellow dots: WSCS dataset; green crosses: stations with collocated PP, R_{rs}, and PAR data. Black solid line boxes: northwest Luzon (L_u, 18°N –20.5°N, 118°E–121°E) and east off Vietnam (V_u, 11°N–15°N, 109°E–111°E) [1].

ioccg.org/groups/Software_OCA/QAA_v6_2014209.pdf) to derive inherent optical properties (IOPs), such as $a(490)$, $b_b(490)$, and $a_{ph}(443)$; they were further fed to the AbPM model [see (4)–(6)] to obtain PP.

Also, in situ measured R_{rs} and PAR were used to estimate daily PP from VGPM [see (1)] and AbPM, with a purpose to evaluate model performances without concerns of issues related to satellite data processing. CbPM was not included in this step because the input parameters for CbPM could not be estimated from R_{rs} [e.g., nitracline depth (Z_{NO3})].

C. In Situ Data

Primary productivity measurements were carried out in three subregions of the SCS (10°N–25°N, 105°E–121°E) between 2009 and 2020, which were mainly located in the NSCS, CSCS, and WSCS parts of SCS (see Fig. 1). PP was measured by the ^{14}C tracer method [39]. A quantum scalar radiometer was used to continuously measure surface PAR (QSPL-2100, Biospherical Instruments Inc., San Diego, CA, USA). Water samples from the 5, 25, 50, and 75 m depth were collected to perform the photosynthesis–irradiance curve (P–E) experiments. Then, the samples were dispensed into 11 or 13 70-mL Corning tissue culture flasks, inoculated with 5–20 μCi of $NaH^{14}CO_3$ solution, and incubated in a photosynthesis simulator on deck for 4 h. After the incubations, the PP was obtained by integrating PP(z) over the day and the euphotic zone. Briefly, the P–E parameters are linearly interpolated in the vertical direction at 6-min time intervals and 1-m depth intervals and then summed up after substitution into PAR and Chl calculations. Detailed information and description regarding PP measurements and its vertical integration in SCS can be found in [2] and [3].

Remote sensing reflectance, R_{rs} (sr^{-1}), which is the ratio of water-leaving radiance to downwelling irradiance just above the surface, was derived after radiometric measurements with a GER 1500 spectroradiometer (Spectra Vista Corporation, Poughkeepsie, NY, USA). For each measurement, three radiances were measured sequentially; they are the upwelling radiance above the surface (L_u, W·m^{-2}·nm^{-1}·sr^{-1}), the radiance from a standard Spectralon plaque (L_{plaque}, W·m^{-2}·nm^{-1}·sr^{-1}), and the downwelling sky radiance (L_{sky}, W·m^{-2}·nm^{-1}·sr^{-1}) in the reciprocal angle of L_u. R_{rs} was then calculated as

$$R_{rs}(\lambda) = \frac{\rho\left(L_u(\lambda) - r \times L_{sky}(\lambda)\right)}{\pi \times L_{plaque}(\lambda)} - \Delta \tag{7}$$

where r is the surface reflectance and a value of 0.023 was taken; ρ is the reflectance of the standard plaque with a reflectance of 0.2 or 0.5; and Δ represents the residual surface contribution (glint and so on), which was determined by assuming $R_{rs}(750) = 0$ (clear oceanic waters) or through an optimization process [40].

Surface water samples (0.1–5 L) were filtered onto 25-mm-diameter glass fiber filters (GF/F, Whatman) for the determination of phytoplankton absorption coefficients and Chl.

The filter pads were stored frozen in liquid nitrogen until after the cruise for analysis. Total particulate absorption coefficient (a_p, m^{-1}) was determined by the transmittance (T)–reflectance (R) filter-pad technique [41], [42] and was measured with a dual-beam PE Lambda 950 spectrophotometer equipped with an integrating sphere (150 mm in diameter). Detrital absorption (a_d, m^{-1}) was then measured after extraction of pigments by methanol, and a_{ph} (m^{-1}) was calculated by subtracting a_d from a_p. Details of the methods can be found in previous work [43]. Chl was measured using high-performance liquid chromatography (HPLC) following the protocol of Huang et al. [44].

To evaluate the PP estimates from satellite measurements by the models described earlier and to increase the number of matchups between satellite and field data, eight-day composite data of Aqua-MODIS were used to match with in situ PP measurements [45], [46]. Note that due to cloud coverage and failures in atmospheric correction [47], only one satellite-in situ data could be matched up if daily satellite products were used.

Gregg and Rousseaux [48], we focused on satellite data in offshore (the bottom depth is deeper than 200 m) waters, whereas the IOPs and Chl products are more reliable than those of nearshore waters due to the impact from river runoff as well as difficulties in obtaining accurate R_{rs} for inshore waters. This is also because coastal waters' spatial heterogeneity is strong and the ocean color products in such waters have higher uncertainties [49].

The matchup strategy follows that described in [50]. Briefly, for each field measurement, 3 × 3 MODIS pixels around this station were extracted. Satellite data were retained only when the valid pixels in the 3 × 3 array were >50% and

TABLE I

MATCHUP STATIONS IN THE SCS SUBREGIONS USED FOR ALGORITHM VALIDATION. N IS THE NUMBER OF MEASURED PP MATCHING UP WITH AVAILABLE MODIS-AQUA PRODUCTS. OBSERVATIONS SHALLOWER THAN 200 M WERE EXCLUDED TO MINIMIZE THE IMPACT OF IMPERFECT SATELLITE PRODUCTS

Sub-region	Cruise	Boreal Season	Date	Long (° E)	Lat (° N)	N	Reference
NSCS	CHOICE-C1	Summer	Jul-Aug 2009	113.1~118.0	18.0~18.6	2	[2]
	CHOICE-C2	Winter	Jan 2010	115.4~120.0	18.8~22.1	6	
	CHOICE-C3	Autumn	Nov 2010	116.0	18.0	1	
	CHOICE-C4	Spring	May 2011	114.8~121.0	18.0~21.8	8	
	NSFC-SCS-DFH11	Summer	Aug 2011	115.5~118.8	20.0	3	
	CHOICE-C5	Summer	Aug 2012	115.5~115.8	20.2~20.5	2	
CSCS	DFH-II	Summer	Jul 2015	111.5	18.0	1	/
	KK1702	Summer	Jun 2017	113.0~116.0	12.0~16.0	4	
	KK1905	Summer	Jul 2017	110.6~116.0	14.0~16.8	2	
	KK2001	Spring	Apr-May 2020	112.0~118.5	10.0~14.0	5	
WSCS	R/V Shiyan-3	Autumn	Sep 2018	110.5~112.5	12.0~14.0	5	[3]

the coefficient of variation (CV) of the valid pixels was less than 0.15 to exclude the errors caused by extreme variations among the pixels. Finally, an average of the remaining pixels was computed and was considered to match up with in situ measurement. From these, a total of 39 data pairs ($N = 39$) were compiled for the evaluation of PP products from satellites obtained by the described models. Table I lists the information of the matchup samples used in this effort.

For these measurements, the coefficient of determination (R^2), root-mean-square difference (RMSD), biased (Bias), and unbiased RMSD (uRMSD) were calculated, all in $\log_{10}$ scale following that in the literature [51], [52], to evaluate the performance of these models:

$$\mathrm{RMSD} = \sqrt{\frac{\sum_{i=1}^{N}\left(\log_{10}(\mathrm{PP}_{\mathrm{est}}(i)) - \log_{10}(\mathrm{PP}_{\mathrm{mea}}(i))\right)^2}{N}} \tag{8}$$

$$\mathrm{Bias} = \overline{\log_{10}(\mathrm{PP}_{\mathrm{est}})} - \overline{\log_{10}(\mathrm{PP}_{\mathrm{mea}})} \tag{9}$$

$$\mathrm{uRMSD} = \sqrt{\left(\mathrm{RMSD}^2 - \mathrm{Bias}^2\right)} \tag{10}$$

where $\mathrm{PP}_{\mathrm{mea}}$ and $\mathrm{PP}_{\mathrm{est}}$ are field-measured PP values and their corresponding estimates, respectively, and N is the number of data pairs.

For comparison between modeled results, we also calculated the unbiased percentage difference (uPD) for each pair of models

$$\mathrm{uPD} = 2 \times (\mathrm{PP}_x - \mathrm{PP}_{\mathrm{AbPM}})/(\mathrm{PP}_x + \mathrm{PP}_{\mathrm{AbPM}}) \times 100 \tag{11}$$

with PP_x representing the PP estimated by the other two models.

D. Other Data and Analysis

To characterize the long-term trends of PP in SCS, linear regression analyses between satellite-derived PP anomalies and other related physical variables were carried out following methods in the literature [48], [53]. A significant trend is defined when the confidence level exceeds 95% ($p < 0.05$).

Meanwhile, in order to extract the principal components accounting for the most dominant interannual variation of PP in different seasons, analysis with empirical orthogonal function (EOF) decomposition, commonly used in the time-series analysis [54], [55], was carried out. As the upper SCS circulation is mainly controlled by the East Asian monsoon and characterized by seasonal upwelling and cold eddies, the seasonal variations of PP mainly appear in winter and summer. Thus, the interannual variations of PP in the SCS in winter and summer were analyzed separately following [56]. First, climatology PP of winter (December–February) and summer (June–August) seasons were calculated. Subsequently, the distributions of PP anomalies (the difference between PP of each season and the climatology) in both winter and summer were obtained. Then, the EOF analysis was applied to the spatial distribution of PP anomalies.

To facilitate analysis and discussion, the monthly mean wind speed data (2003–2019) from cross-calibrated multiplatform (CCMP) were used in the study, which was produced by Remote Sensing Systems (https://remss.com/measurements/ccmp/). In addition, monthly averaged Chl products by the ocean color index (OCI) algorithm and monthly mean SST data were also downloaded from NASA, with a spatial resolution of 9 km.

III. RESULTS

A. Comparison of Modeled PP With in Situ PP

To characterize the performance of these PP models, we first used in situ data [R_{rs} and PAR(0)] to estimate daily PP and compared the results with that from incubation measurements. Fig. 2 shows the scatterplots between estimated PP and measured PP and Table II tabulates the statistics. PP from 20 stations (in the NSCS, see Fig. 1, green crosses) with concurrent field measurements [including PP, R_{rs}, and PAR(0)] were compiled since there were no in situ R_{rs} for the CSCS and WSCS cruises. Overall, the two models had R^2 values in the range of 0.43–0.54, with a Bias between −0.01 and −0.18, while uRMSD (0.21) was the same for

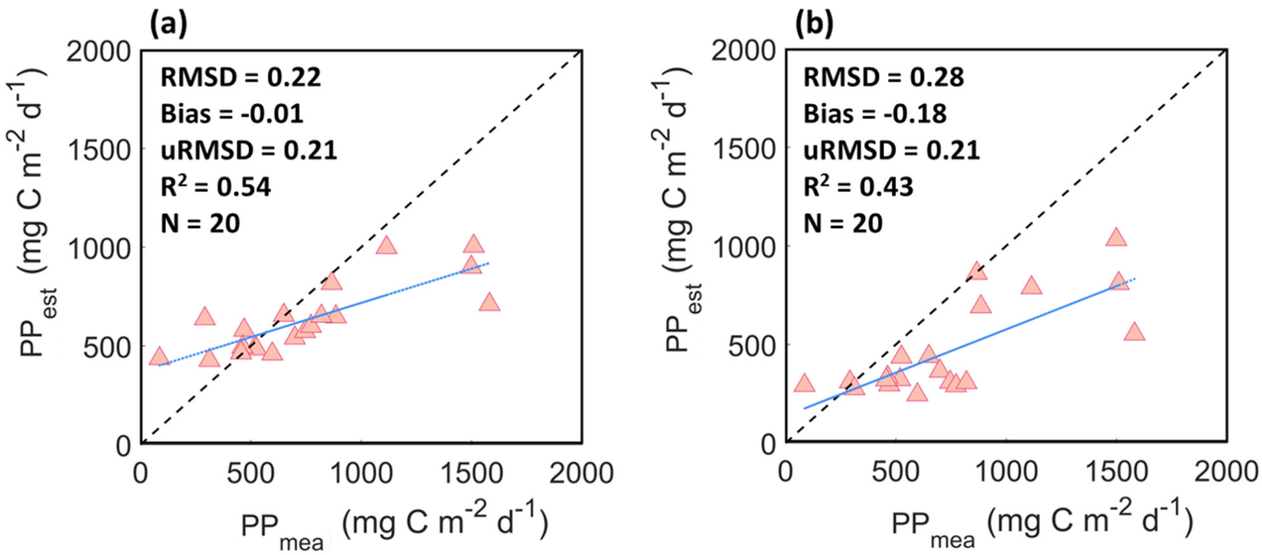

Fig. 2. Comparison between in situ (PP_{mea}) and model-estimated (PP_{est}) primary production, where field data were used as model inputs. (a) AbPM. (b) VGPM. The black dashed line is the 1:1 line, whereas the blue line represents the regression line.

TABLE II
SUMMARY OF STATISTICS OF PP MODEL PERFORMANCES FOR MATCHUP STATIONS

Model inputs	Model	RMSD	Bias	uRMSD	slope	R^2	N
in situ R_{rs}&PAR	VGPM	0.28	-0.18	0.21	0.44	0.43	20
	AbPM	0.22	-0.01	0.21	0.35	0.54	
MODIS and other	VGPM	0.29	-0.15	0.24	0.35	0.26	39
	CbPM	0.34	0.21	0.26	0.32	0.15	
	AbPM	0.22	0.06	0.21	0.47	0.47	

the two models. Compared with in situ PP that ranged in 86–1581 $mg{\cdot}C{\cdot}m^{-2}{\cdot}d^{-1}$, VGPM and AbPM did not provide highly consistent estimates, where both models underestimated PP at the high end and overestimated PP at the lower end. Although the outcome of AbPM appeared slightly better when compared to in situ measured data, due to the small number of samplings, it is inconclusive if AbPM is better from this dataset nor conclusive if there are more uncertainties in the measured PP or modeled PP.

We further compared the PP estimates obtained from satellite data by the three models with field-measured PP, where 39 matchups were compiled as mentioned in Section II-C, with scatterplots presented in Fig. 3 for visual inspection, while statistics are included in Table II. Note that the PP results of VGPM and CbPM were downloaded from the website of model developers.

Table III summarizes an evaluation of the individual components (e.g., R_{rs}, PAR(0), and SST) used in these models, where the performance is in general consistent with that presented in the literature [57], [58], [59], [60]. The lower R^2 value for PAR(0) is due to a very narrow range of values (35.2–56.7 $mol{\cdot}photons{\cdot}m^{-2}{\cdot}d^{-1}$) for these low-latitude waters.

Among the three models evaluated, the R^2 values are in a range of 0.15–0.47, slightly worse than using in situ R_{rs} and PAR(0). This is mainly attributed to no precise matchups between satellite pixels and in situ measurements due to different footprint and temporal coverage. Similarly, as the above evaluation among in situ measurements, AbPM showed the highest R^2 (0.47) and lowest uRMSD (0.21). In comparison, VGPM generally shows an underestimation, while CbPM shows an overestimation. For this dataset ($N = 39$), AbPM explained 47% of the PP variability, where in situ measured PP is in a range of 100–1315 $mg{\cdot}C{\cdot}m^{-2}{\cdot}d^{-1}$, and again, VGPM and AbPM showed lower estimates at the high end of PP measurements. Reasons for these discrepancies include measurement uncertainties, satellite data processing, as well as the far from perfect "matchup" between satellite and in situ data. More discussion regarding model uncertainties can be found in the literature [30], [61], [62] and the following. Nevertheless, previous round-robin comparisons of primary productivity algorithms [25], [51] showed that the R^2 values of 30 models were in a range of 0.23–0.60 with a mean value of 0.51 ± 0.01, which suggests that the outcome of AbPM is still at the higher end for such comparisons.

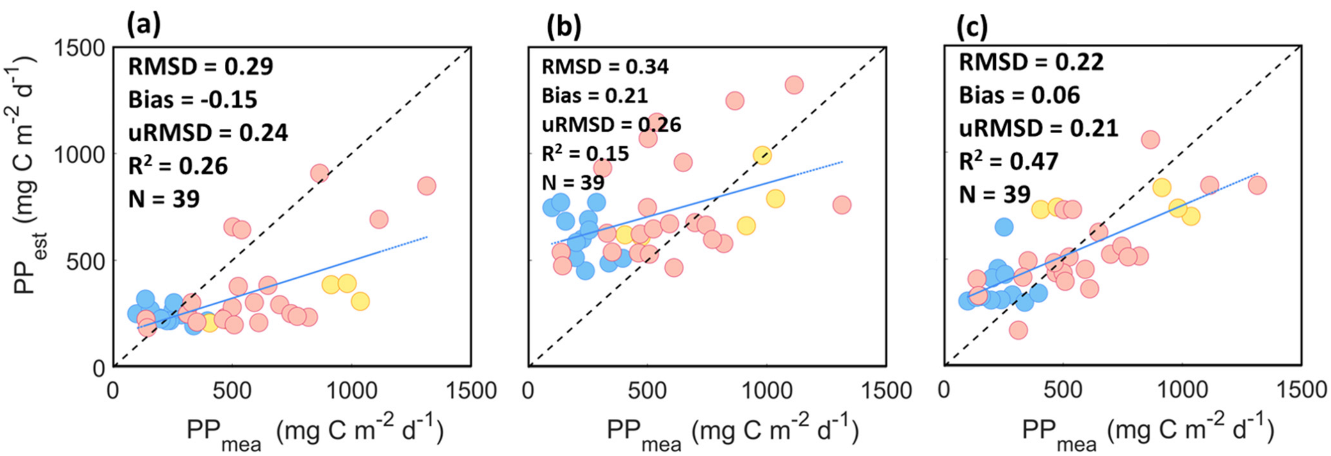

Fig. 3. Comparison between in situ (PP_{mea}) and model-estimated (PP_{est}) primary production, where satellite and other environmental data were used as model inputs. (a) VGPM. (b) CbPM. (c) AbPM. The black dashed line is the 1:1 line, whereas the blue line represents the regression line.

TABLE III
SUMMARY OF STATISTICS OF CORRELATION COEFFICIENT OF LINEAR REGRESSION, RMSD, uRMSD, AND NUMBER OF MATCHUP POINTS FROM THE THREE SUBREGIONS

Input variables	RMSD	Bias	uRMSD	R^2	N		
					NSCS	CSCS	WSCS
$R_{rs}(412)$	0.07	0.03	0.06	0.94	8	/	/
$R_{rs}(443)$	0.07	0.02	0.07	0.88	8	/	/
$R_{rs}(490)$	0.05	0.01	0.05	0.75	8	/	/
PAR	0.08	0.02	0.08	0.28	8	/	/
SST	0.01	0.01	0.01	0.92	22	/	5
Chl	0.18	-0.10	0.14	0.75	22	/	5
$a_{ph}(443)$	0.09	-0.04	0.08	0.85	15	/	5

B. General Spatial Characteristics

The above validations regarding the three PP strategies and models suggested that AbPM provided better results for PP remote sensing; therefore, values from AbPM were used to describe the general spatial variations of PP in the SCS basin (for depths deeper than 200 m). The spatial distribution of climatological PP (for the period of 2003–2019) is presented in Fig. 4, which is highly season dependent. Generally, AbPM captures the basic distribution features of PP levels being high in the upwelling areas and low in the basin area, with the highest PP levels in winter and the lowest in summer (Fig. 4). PP peak occurs in the northwestern part of Luzon in winter and is about two times higher than that in the central basin area. For the entire SCS basin, its annual average is 503 ± 34 mg·C·m^{-2}·d^{-1} (~252 Tg·C·yr^{-1}). The highest productivity is in winter with an average of 526 ± 17 mg·C·m^{-2}·d^{-1}, followed by spring (506 ± 13 mg·C·m^{-2}·d^{-1}) and autumn (492 ± 7 mg·C·m^{-2}·d^{-1}), with the lowest in summer (482 ± 3 mg·C·m^{-2}·d^{-1}). These results are similar to that observed by Chen et al. [63] based on limited field data. In addition, the winter estimates (~546 mg·C·m^{-2}·d^{-1}) by AbPM are found consistent with those reported in [64] (~530 mg·C·m^{-2}·d^{-1}) from field measurements, suggesting that the seasonal variations of PP in SCS obtained from AbPM are reasonable.

There existed a zone of surge-type high PP along the Vietnamese shore in summer, with productivity reaching ~600 mg·C·m^{-2}·d^{-1} [Fig. 4(b)]. This effect further extends to the central part of the basin in autumn, showing a trend of high PP distribution in the west and low PP in the east. This is related to the prevailing southwest monsoon and high rainfall in summer, which caused the injection of land-sourced water carrying large amounts of nutrients into the ocean, resulting in a significant increase in PP in WSCS [65].

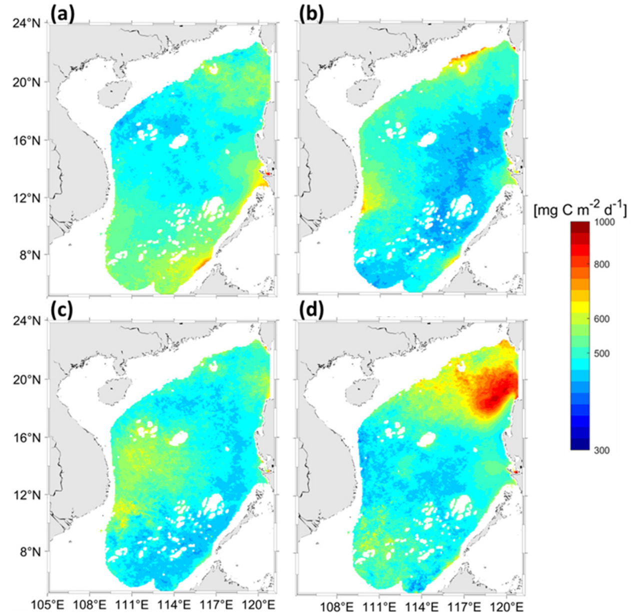

Fig. 4. Spatial distribution of AbPM-obtained seasonal climatology PP of SCS from 17 years (from January 2003 to December 2019) of satellite measurements. (a) Spring (March–May, MAM). (b) Summer (June–August, JJA). (c) Autumn (September–November, SON). (d) Winter (December–February, DJF).

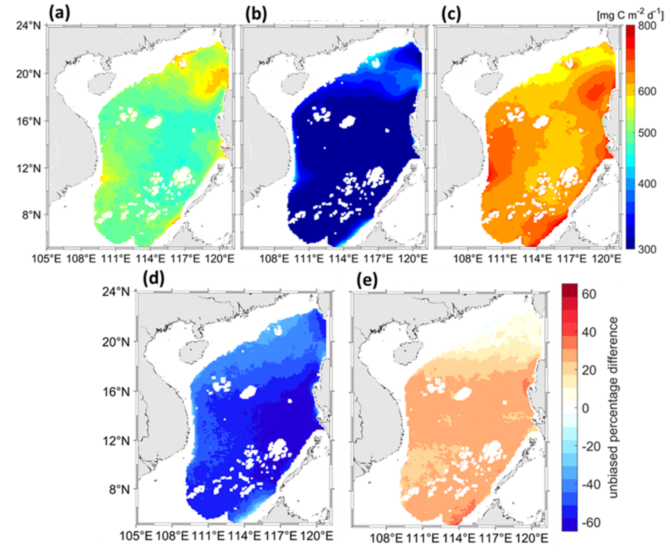

Fig. 5. Spatial distribution of annual climatology PP ($mg{\cdot}C{\cdot}m^{-2}{\cdot}d^{-1}$) generated by three different PP models with MODIS data obtained from 2003 to 2019. (a) AbPM. (b) VGPM. (c) CbPM. (d) and (e) uPD of VGPM and CbPM compared to AbPM, respectively.

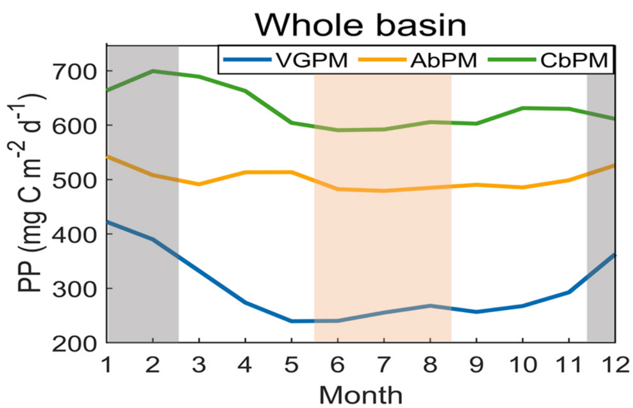

Fig. 6. Monthly climatology PP of SCS basin from the three models obtained from MODIS measurements. Gray shadow refers to winter (December–February); orange shadow refers to summer (June–August).

In wintertime [Fig. 4(d)], due to the intensification of winter mixing, a patch of extremely high PP values forms in northwestern Luzon (a mean value up to 800 $mg{\cdot}C{\cdot}m^{-2}{\cdot}d^{-1}$). In addition, a secondary strong patch exists in the southern part of the SCS centered around 111°E, 8°N. PP data from field measurements also show winter peaks mainly in northwestern Luzon (>500 $mg{\cdot}C{\cdot}m^{-2}{\cdot}d^{-1}$), the basin region of the SCS, and the Sunda shelf [9]. Overall, the pattern of PP exhibits clear strong spatial and seasonal variations.

Because of the different strategies in estimating PP from remote sensing data, the climatological (2003–2019) spatial pattern of PP from AbPM is different from that obtained with VGPM and CbPM [see Fig. 5(b) and (c)], where overall PP from VGPM is ~50% lower than that from AbPM [Fig. 5(d)], while the PP from CbPM is ~40% higher [Fig. 5(e)]. These results further highlight the dependence of basin-scale PP products on the models of PP from satellite data.

C. General Temporal Characteristics

For the temporal (monthly climatology) variability of the entire basin, as shown in Fig. 6, AbPM exhibits the highest value in winter (January) and the lowest in summer (July), but the difference is just about 11%. The winter high and summer low in PP are also observed from the results of CbPM and VGPM, but the monthly variation is not the same, where CbPM shows high PP in February and March and October and November, and VGPM obtained a small PP bump in August. More importantly, while both AbPM and CbPM show mild monthly variations, the winter high PP from VGPM is nearly 1.7 times that of its summer low, i.e., a significantly stronger monthly (or seasonally) variation from VGPM. The above results indicate that there are considerable differences in temporal patterns among the PP results obtained from different models.

These model dependences also appeared at the upwelling zones (see Fig. 7 for examples), where high PP often emerges due to enhanced water mixing and nutrient enrichment [11], [63], [65]. For the upwelling zone off Vietnam (Fig. 7(a), see Fig. 1 for locations), while all three PP models showed summer high PP, but VGPM obtained the maximum in winter, not in summer as that indicated by results from AbPM and CbPM as well as from field observations [9]. On the other hand, for the upwelling zone of Luzon Strait [Fig. 7(b)], although the three models exhibit similar seasonal PP cycles of high in winter and low in summer, the VGPM model resulted in significantly lower values in summer and much stronger seasonal variations.

D. Model Analysis From EOF

The model-dependent variations of SCS PP at various scales make it difficult to conclude results from which model is closer to reality. To address this question, we decomposed the observed long-term spatiotemporal PP anomaly field with EOF analysis and compared the results with known understandings

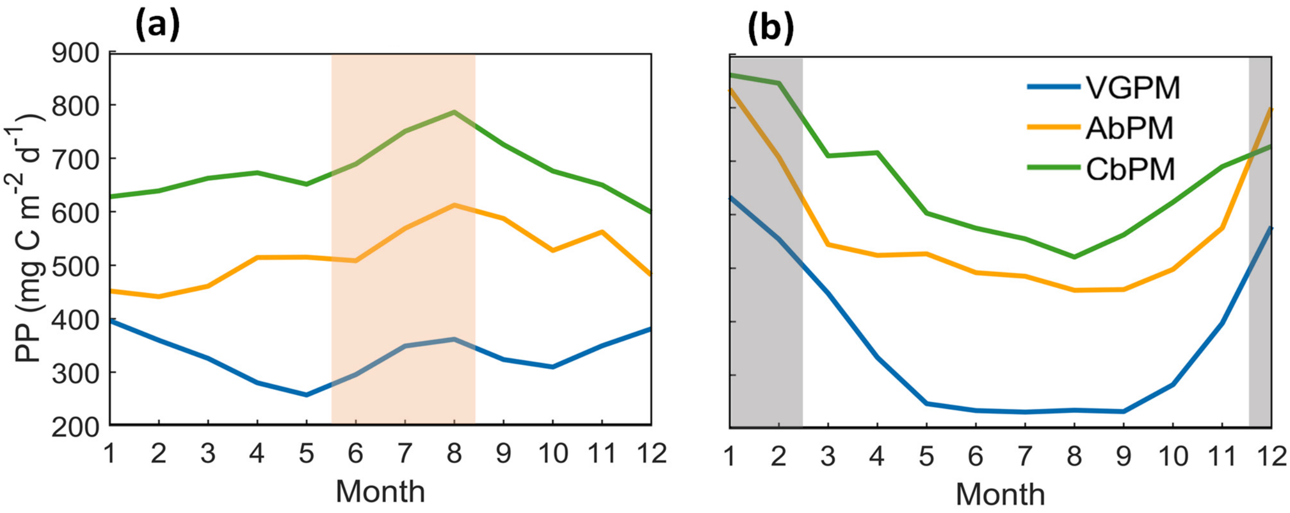

Fig. 7. Monthly climatology PP of the two well-known upwelling zones in SCS from the three models obtained from MODIS measurements. (a) V_u. (b) L_u. Shadow colors are the same as that in Fig. 6.

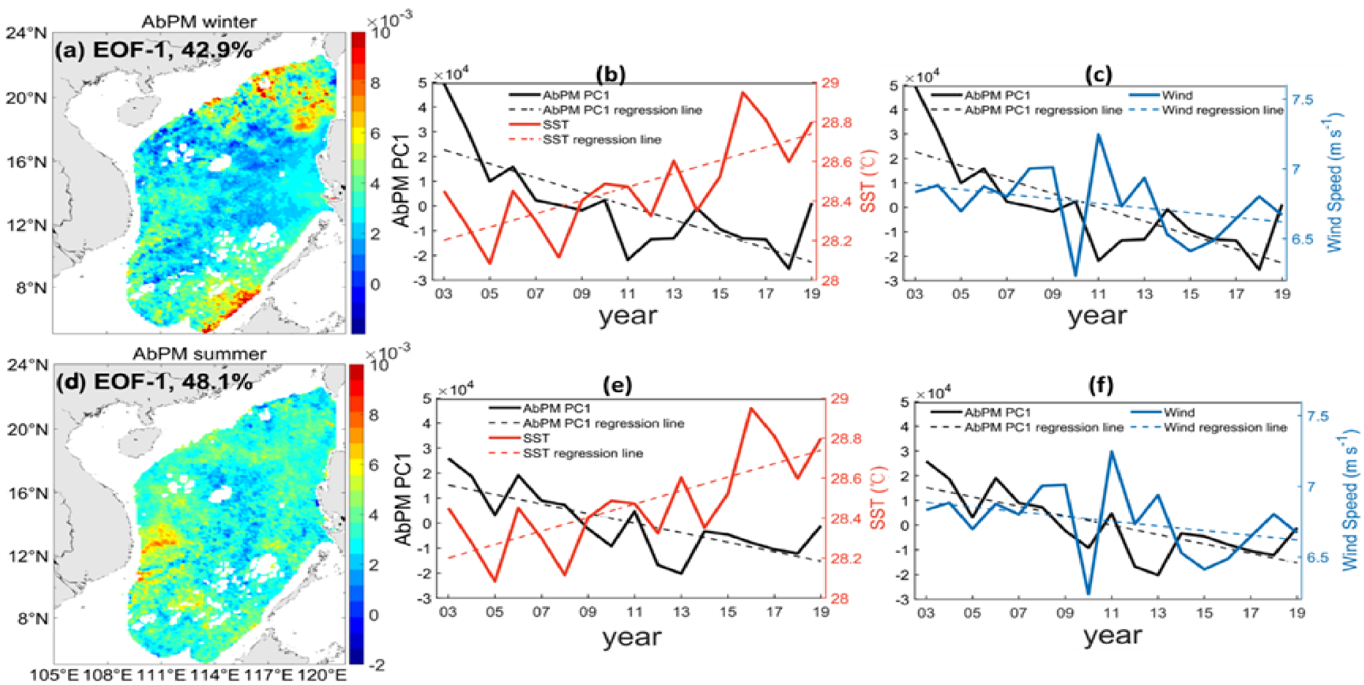

Fig. 8. (a) Spatial variation of the first mode of EOF analysis for winter (December–February) SCS PP obtained by AbPM. (b) and (c) Annual variation of the PC1 (left axis) of the first EOF mode in winter and its relationship with SST (red curve, right axis) and wind speed (blue curve, right axis). (d)–(f) are the same as (a)–(c), but for summer SCS PP (June–August).

of SCS productivity. The results are shown in Figs. 8–10. It is found that the first EOF mode of AbPM-estimated PP accounted for 43% and 48% of the PP spatial variance in winter and summer, respectively, describing a large fraction of the PP variations [Fig. 8(a) and (d)]. The corresponding spatial patterns of this EOF mode indicate spatially different response of PP to environmental forcings, where higher values are apparent for waters off Luzon in winter and another off Vietnam in summer. These patches were exactly consistent with the well-known upwelling zones, i.e., the winter Luzon bloom [66], [67] and summer Vietnamese coastal bloom [65], [68]. The behavior of this mode in the time domain is further represented by its principal component 1 (PC1) [Fig. 8(b), (c), (e), and (f)], where a significant decreasing trend for the period of 2003–2019 (-15.0% yr^{-1} for winter, $p < 0.05$; -14.7% yr^{-1} for summer, $p < 0.05$) emerged. This PP variability from AbPM estimates is a response to the interannual variations of both wind and SST for this period [Fig. 8(b), (c), (e), and (f)], with wind (SST) decreased (increased) by -3.9% yr^{-1} (1.9% yr^{-1}). The decrease (increase) of wind (SST) would result in less nutrient due to relaxed mixing in the water column, thus a decrease in primary production. These results echo the findings of Shih et al. [60] from the time-series study conducted at the South East Asian Time-series Study (SEATs) that climate warming (increased SST) has led to a decrease in phytoplankton primary production in low-latitude waters such as the SCS.

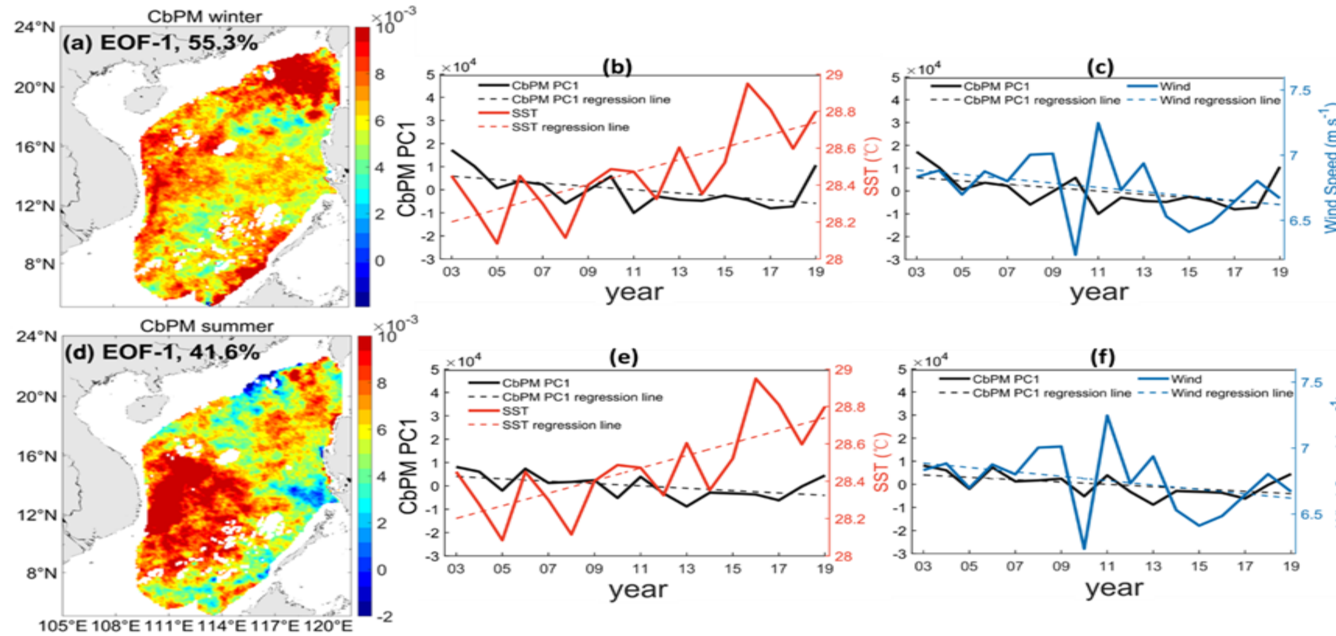

Fig. 9. Same as Fig. 8, but for CbPM-estimated PP in SCS. (a) Spatial variation of the first mode of EOF analysis for winter (December–February) SCS PP obtained by CbPM. (b) and (c) Annual variation of the PC1 (left axis) of the first EOF mode in winter and its relationship with SST (red curve, right axis) and wind speed (blue curve, right axis). (d)–(f) are the same as (a)–(c), but for summer SCS PP (June–August).

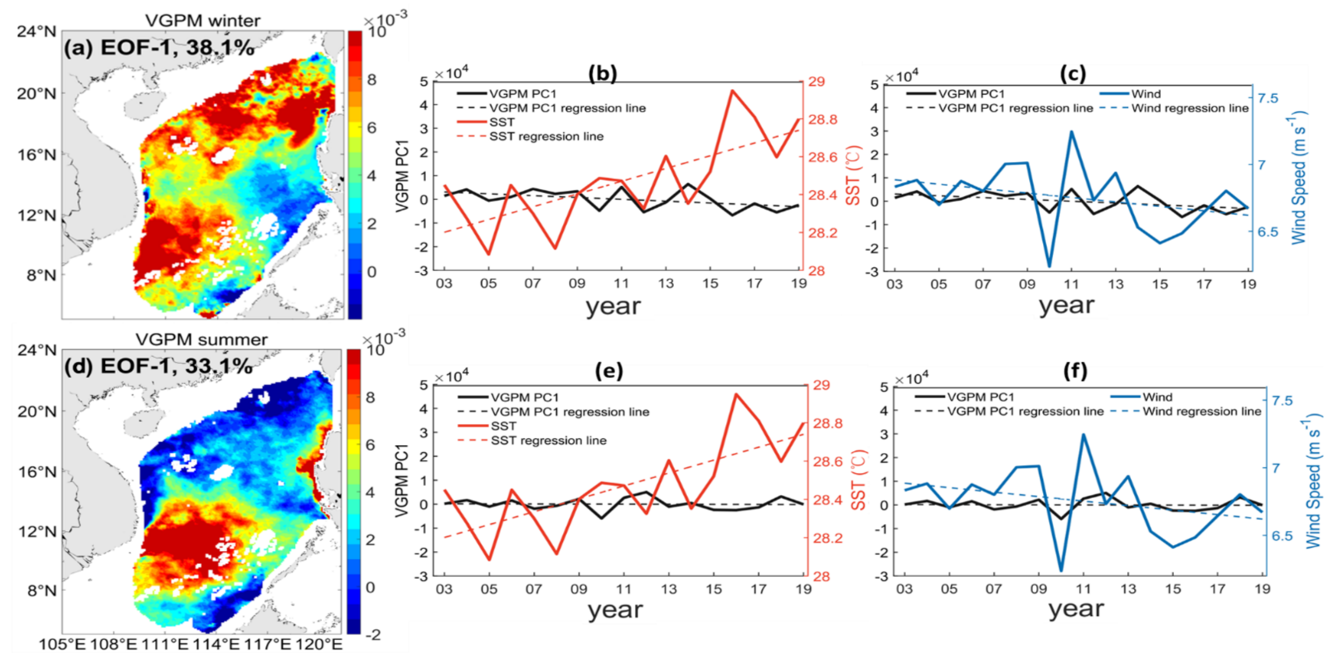

Fig. 10. Same as Fig. 8, but for VGPM-estimated PP in SCS. (a) Spatial variation of the first mode of EOF analysis for winter (December–February) SCS PP obtained by VGPM. (b) and (c) Annual variation of the PC1 (left axis) of the first EOF mode in winter and its relationship with SST (red curve, right axis) and wind speed (blue curve, right axis). (d)–(f) are the same as (a)–(c), but for summer SCS PP (June–August).

On the other hand, the first EOF mode of PP from VGPM and CbPM estimates (Figs. 9 and 10) does not show clear relationships with the main oceanographic features of this region. For instance, the winter high of the first EOF mode for both CbPM and VGPM [see Figs. 9(a) and 10(a)] appears not only for waters off Luzon but also in the broad east coast of Vietnam, but there is rare evidence in the literature on a high productivity off the Vietnamese coast in winter. On the other hand, for both CbPM and VGPM, the summer high of the first EOF mode extends well into the southern SCS and the SCS basin, which is neither supported by the circulation dynamics of the summer upwelling off the Vietnamese coast. In addition, while the PC1 of the first EOF mode of CbPM also shows decreasing trends of -9.8% yr^{-1} ($p < 0.05$) for winter and -10.2% yr^{-1} ($p < 0.05$) for summer, which are weaker compared to those of AbPM. Furthermore, there is no strong trend for PC1 of the first EOF model of VGPM (-9.6% yr^{-1} for winter, $p = 0.05$; -0.7% yr^{-1} for summer, $p = 0.89$) estimates. From these results and comparisons, it suggests that PP from AbPM reflects better the spatiotemporal variations of PP in SCS and the responses to environmental forcings.

IV. Discussion

A. Major Reasons for Model-Measurement Discrepancies

The performance of the PP models shown in Section III-A, as well as those shown in the round-robin comparisons of PP algorithms [25], [51], either with measured data or with satellite data as inputs, indicates that there are quite large differences between measured and modeled PP, even for the better performing AbPM model. The reasons behind the discrepancies are multifold. When using in situ data as input, part of the low performance is in the uncertainties of the measurements (see Fig. 2). For instance, between Stations K1 and S1 (see Fig. 1 for locations), field measured PAR, $a_{ph}(443)$, and Chl are similar (Chl values were within a factor of ∼1.5, and others were within a factor of 1.2), but in situ PP differed by a factor of ∼5, which then contributed significantly to the differences between estimated PP and modeled PP. Another factor is the on-deck ^{14}C incubation for PP measurement with flowing surface water to maintain temperature, a scheme taken since the joint global ocean flux (JGOFS) program in the 1990s [69], [70]. Such an approach inevitably could lead to the possibility that deep phytoplankton was growing at unsuitable temperatures, especially those samples from 50 and 75 m with elevated chlorophyll values, where the temperature could be 3 °C–5 °C lower compared to that at surface. Consequently, this will cause uncertainties in the measured PP. On the other hand, because most of the photosynthesis happens near surface, phytoplankton at deeper depths contribute just ∼5%–30% to the water-column-integrated PP in SCS, and such uncertainties due to temperature difference are considered acceptable since JGOFS. In addition to the measurement errors or uncertainties, another key source of discrepancy between satellite and in situ data is the mismatch in time and space, where in situ data represent a point measurement within a day, while satellite data represent an average of an area in square kilometers for a period of eight days. Unfortunately, limited by field capacities and techniques to obtain in situ PP as well as the spatial resolution of ocean color satellites, as shown in many similar studies [71], [72], [73], [74], it is not possible yet to obtain a large number of perfect matchups between satellite and in situ data.

B. AbPM

One of the major components for AbPM is the phytoplankton absorption coefficient (a_{ph}), which is a strong predictor for phytoplankton biomass [59], [75]. Because a_{ph} is a key component for the estimation of PP via AbPM [see (4)], its accuracy plays an important role on the robustness of PP estimation. For the field data compiled for this study, it is found that there is an excellent agreement between field-measured and satellite R_{rs}-inverted $a_{ph}(443)$ [$R^2 = 0.85$, uRMSD = 0.08, and $N = 20$, see Table III and Fig. 11(a)], with estimates from R_{rs} distributed around the 1:1 line from pad-measured $a_{ph}(443)$. This result echoes earlier findings that ocean color inversion can obtain highly accurate a_{ph} [76], [77], [78], which in part is because a_{ph} is an optical property that is directly related to R_{rs} [79], [80].

The second major component for AbPM is the quantum yield (ϕ) of photosynthesis, which is not a property directly retrievable by remote sensing yet, but modeled with two parameters (ϕ_m and K_ϕ), with their values obtained from various field measurements [35], [62], [81]. Among them, the effect of K_ϕ on the AbPM-estimated PP is mainly in the surface layer, where it varies between 5 and 15 mol·photons·m^{-2}·d^{-1} [38], while ϕ_m is more influenced by both depth and nutrient levels and varies roughly between 0.005 and 0.08 mol·C·mol·photons^{-1} [2], [82], with its lowest value usually in the surface layer and under oligotrophic regimes [83], [84]. In principle, ϕ_m and K_ϕ should not be constants. However, since these parameters cannot be accurately determined yet from remote sensing, the default and constant values used in this study were taken from [35]. Although $\phi_m =$ 0.06 mol·C·mol·photons^{-1} works overall reasonably well for the SCS basin, the validation results with measured data still show underestimation at high values and overestimation at low values [see Fig. 3(c)], if we assume that field measured PP is accurate. This is mainly because the uncertainty of ϕ_m has the greatest impact on the output of AbPM (∼38%) [85]. Even so, the results of this study are similar to that obtained in [22] with the modified VGPM ($R^2 = 0.49$ and $N = 13$), also for waters of the SCS.

C. VGPM

Concentration of chlorophyll (Chl) is a key input in VGPM. Even though highlighted in [28] that Chl is a poor proxy for phytoplankton biomass in the ocean as it can be strongly influenced by the physiological state of the phytoplankton assemblage, Chl is a common input for most PP models. In this study, the satellite-estimated Chl matched in situ measurements quite well [$R^2 = 0.75$ and $N = 27$; see Table III and Fig. 11(b)], with a uRMSD value as 0.14. This suggests that the underestimation PP (bias = −0.15) at the high end (>500 mg·C·m^{-2}·d^{-1}) by VGPM is not caused by errors in Chl derived from satellite measurements, if field measured PP is reliable. This point is echoed when using the measured Chl as the input (Bias = −0.18).

The other key component for VGPM is P^B_{opt}, where a range of 4.00–6.54 mg·C (mg·Chl)$^{-1}$·h^{-1} was obtained based on the scheme of Behrenfeld and Falkowski [16] for a temperature range of 17 °C–32 °C. These modeled P^B_{opt} were quite low compared to in situ P^B_{opt} (slightly under 20 mg·C (mg·Chl)$^{-1}$·h^{-1}) for a similar temperature range [26]. In other words, a significant underestimation of the modeled P^B_{opt} contributes most to the underestimation of the high end of the VGPM-estimated PP. Certainly, the model for P^B_{opt} could be improved with other inputs or math formula, but such revisions are always data-dependent, where its applicability in a wider range of environments and time spans is unsure. Furthermore, the reason P^B_{opt} has such poor accuracy is, ultimately, because in VGPM, it is expressed only as a single environmental variable SST, even though the satellite SST can be a good reflection of the measured SST ($R^2 = 0.92$, uRMSD = 0.01, and $N = 27$; see Table III). However, in many cases, SST is

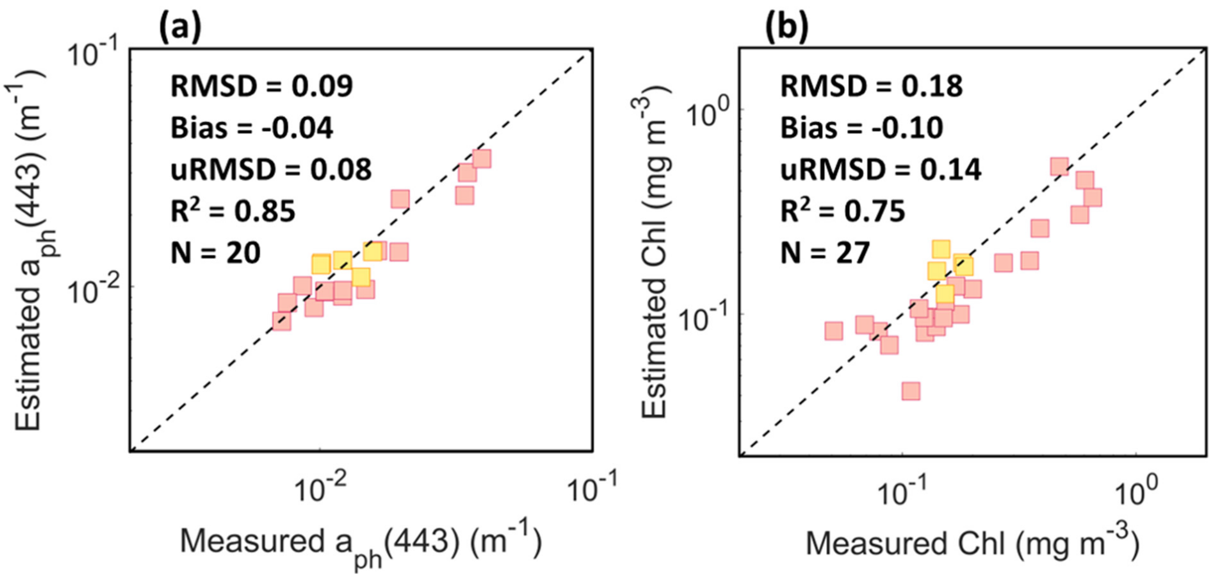

Fig. 11. Comparison between properties estimated from R_{rs} and measured from water samples for (a) $a_{\rm ph}(443)$ and (b) Chl. Red and yellow squares are for NSCS and WSCS, respectively. The black dashed line is the 1:1 line.

far less important than the effect of nutrients on phytoplankton carbon fixation [28], [29], [86]. In addition, part of the variation of $P^B_{\rm opt}$ is driven by the chlorophyll-specific absorption coefficient ($a_{\rm ph}*$) [27], which can vary more than fourfold for the same Chl due to pigment composition and "packing effects" [87], [88], [89]. Such a large range of variation will greatly increase the probability that $a_{\rm ph}*$ (and then $P^B_{\rm opt}$) does not match the PP model and ultimately leads to errors in the estimated PP [30].

D. CbPM

For CbPM, phytoplankton carbon biomass ($C_{\rm ph}$) is one of the key inputs, which likely contributed mainly to the overprediction of PP at the lower end (Fig. 3(b), blue circles), if we assume that field-measured PP is accurate and no gaps in satellite-field matchups. This is because $C_{\rm ph}$ is derived from $b_{\rm bp}(440)$, which includes the contributions from phytoplankton and others (e.g., suspended sediments, detritus, and bubbles) when it is estimated from ocean color. Therefore, only a portion of $b_{\rm bp}(440)$ can be considered for phytoplankton biomass, and this portion could be quite small when there are large amounts of nonalgal particles in the water column. Certainly, such portions will vary from water to water, where the global constant value (0.00035 $\rm m^{-1}$) used in (3) could not be universal [90]. If a value of 0.00056 $\rm m^{-1}$ proposed for the SCS [91] was applied, $C_{\rm ph}$ would be dropped to 7.7 ± 4.1 $\rm mg{\cdot}m^{-3}$ from 18.5 ± 5.8 $\rm mg{\cdot}m^{-3}$ for this dataset, indicating the importance and challenge to accurately estimate $C_{\rm ph}$ from $b_{\rm bp}$, even assuming that $b_{\rm bp}$ can be inverted robustly from $R_{\rm rs}$, but always, there are various levels of uncertainties [80], [92].

Another critical input for CbPM is the Chl:$C_{\rm ph}$ ratio, which tracks the change of phytoplankton physiological status [28], [93] and is used to estimate the growth rate of phytoplankton [28], [29]. This Chl:$C_{\rm ph}$ ratio is described as a function of PAR, the diffuse attenuation coefficient, and the mixed-layer depth [94], where the accuracy of Chl:$\rm C_{ph}$ ratio for SCS is not known.

E. PAR at Surface

A common input parameter used in all primary product models is the ambient light intensity (PAR), where the standard daily PAR product provided by NASA has uncertainties in the range of 10%–30% [95]. When the time scale is stretched to monthly averages, the short-term variability affected by cloud cover and other factors is reduced, and the uncertainty of the monthly PAR is dropped to about 6% [96]. In this study, the agreement between in situ PAR(0) and satellite PAR(0) is far from exciting ($R^2 = 0.28$, uRMSD = 0.08, and $N = 8$) due to the small number of matchups and one "outlier," and the statistics improved significantly if this outlier was removed ($R^2 = 0.82$, uRMSD = 0.03, and $N = 7$). Overall, in view of the large differences between the modeled and measured PP, as indicated in earlier studies [16], [25], [26], uncertainties in PAR(0) are a minor source of error for the estimation of PP.

F. Forcing for the Decreasing PP in the Upwelling Zones

The mode analysis in Section III-D suggested basin wide declines in PP, which were more significant in the upwelling systems. This implies common but inhomogeneous large-scale forcing imparted on the SCS. In recent decades, the continuous warming of the ocean [97] and the weakening of wind were observed due to climate changes. Both factors intensified the near-surface stratification [98] and can be the driver of such decline. Indeed, the SST (wind) showed an antiphase (in-phase) fluctuation with the PC1 [Fig. 8(b), (c), (e), and (f)]. The SST of SCS in recent decades has witnessed a warming rate at ∼0.5 °C per decade, combined with the wind speed declines and deteriorating nutrient supply provided by mixing. Moreover, the upwelling systems were more sensitive to such forcing, leading to more significant declines therein [47]. However, a more complex mechanistic analysis is beyond the scope of our current study. In general, the results here show that PP from AbPM better highlights the role of climate oscillations, more reasonable on the temporal variability. These explanations are consistent with the findings obtained from SEATs station in the SCS [99], [100], where Shih et al. [60] showed a negative and statistically significant correlation between in situ PP and in situ SST from 14 years (2003–2016) of time-series measurements. They concluded that the observed overall decrease in in situ PP could be partially explained by an increase in SST. It is necessary to keep in mind that even though we found the long-term (∼20 years) trends in PP, this is far from sufficient to predict the response of marine ecosystems in a future warming climate. This is on account of the phytoplankton's physiological properties exhibiting complex, nonlinear responses to changes in temperature, light, and nutrients. Undeniably, this knowledge is critical to better predict the effects of climate change on ecosystems and carbon fluxes.

V. CONCLUSION

It has been a long-standing challenge and question on which PP model should be applied to satellite data products for obtaining basin-scale estimates of PP, as this is a prerequisite for the characterization and evaluation of the spatial distribution and temporal variation of PP over large regions. For the SCS waters, existing knowledge regarding the PP variation has been derived from the VGPM (or its variant) model; apparently, due to the inherent uncertainties associated with VGPM, our results suggest that some of the earlier findings and conclusions deserve serious revisions. Furthermore, for the three models (VGPM, CbPM, and AbPM) applied and evaluated in this study, AbPM (a model centered on phytoplankton absorption) presented more reasonable results compared to field measurements and understanding of phytoplankton response to environmental forcings. These include overall basin-scale higher PP in winter and lower PP in summer, as well as upwelling-induced high PP off Luzon in winter and off Vietnam in summer. Furthermore, due to weakening winds and warming in the SCS, there is a clear decreasing trend in the AbPM-estimated PP in the upwelling zones from 2003 to 2019 (-15.0% yr^{-1} for winter, $p < 0.05$; -14.7% yr^{-1} for summer, $p < 0.05$), a feature not well captured by the PP results estimated from VGPM and CbPM. The results from this effort not only provide new, more reliable, insights on the spatial and temporal variations of PP in SCS but also echo that AbPM is a plausible scheme for the estimation of PP using ocean color satellite products, where further efforts should be focused on improving the estimation of the quantum yield of phytoplankton photosynthesis (ϕ), as well as methods to obtain more accurate field measurements of PP.

ACKNOWLEDGMENT

The authors would like to thank Dr. Yuyuan Xie and Dr. Jie Xu for providing valuable data used in this study. CCMP Version-3.0 analyses produced by the Remote Sensing Systems (data are available at www.remss.com) are greatly appreciated. All satellite data used in this study are available from NASA (https://oceancolor.gsfc.nasa.gov/) (http://hahana.soest.hawaii.edu/hot/) or the Oregon Ocean Productivity Laboratory (OSU: http://sites.science.oregonstate.edu/ocean.productivity/index.php). The in situ primary production data are archived in the NCEI World Ocean Database (https://data.nodc.noaa.gov/cgi-bin/iso?id=gov.noaa.nodc:0211060#). Comments and suggestions from two anonymous reviewers greatly improved this manuscript.

REFERENCES

[1] K.-K. Liu, S.-Y. Chao, P.-T. Shaw, G.-C. Gong, C.-C. Chen, and T. Y. Tang, "Monsoon-forced chlorophyll distribution and primary production in the South China Sea: Observations and a numerical study," *Deep Sea Res. I, Oceanographic Res. Papers*, vol. 49, no. 8, pp. 1387–1412, Aug. 2002.

[2] Y. Xie et al., "Photosynthetic parameters in the northern South China Sea in relation to phytoplankton community structure," *J. Geophys. Res., Oceans*, vol. 120, no. 6, pp. 4187–4204, 2015, doi: 10.1002/2014jc010415.

[3] J. Liao, J. Xu, R. Li, and Z. Shi, "Photosynthesis-irradiance response in the eddy dipole in the western South China Sea," *J. Geophys. Res., Oceans*, vol. 126, no. 5, May 2021, Art. no. e2020JC016986, doi: 10.1029/2020jc016986.

[4] C. B. Field, M. J. Behrenfeld, J. T. Randerson, and P. Falkowski, "Primary production of the biosphere: Integrating terrestrial and oceanic components," *Science*, vol. 281, no. 5374, pp. 237–240, Jul. 1998.

[5] P. G. Falkowski, E. A. Laws, R. T. Barber, and J. W. Murray, "Phytoplankton and their role in primary, new, and export production," in *Ocean Biogeochemistry: A synthesis of the Joint Global Ocean Flux Study*, M. J. Fashman, Ed. Berlin, Germany: Springer, 2003, pp. 99–121.

[6] A. J. Watson and J. C. Orr, "Carbon dioxide fluxes in the global ocean," in *Ocean Biogeochemistry*, M. J. R. Fasham, Ed. Berlin, Germany: Springer, 2003, pp. 123–143.

[7] F. P. Chavez, M. Messié, and J. T. Pennington, "Marine primary production in relation to climate variability and change," *Annu. Rev. Mar. Sci.*, vol. 3, no. 1, pp. 227–260, Jan. 2011.

[8] M. J. Behrenfeld et al., "Climate-driven trends in contemporary ocean productivity," *Nature*, vol. 444, pp. 752–755, Dec. 2006, doi: 10.1038/nature05317.2006.

[9] X. Ning, "Physical-biological oceanographic coupling influencing phytoplankton and primary production in the South China Sea," *J. Geophys. Res.*, vol. 109, no. C10, pp. 1–20, 2004, doi: 10.1029/2004JC002365.

[10] N. Z. Jiao et al., "Carbon pools and fluxes in the China seas and adjacent oceans," *Sci. China-Earth Sci.*, vol. 61, no. 11, pp. 1535–1563, Nov. 2018, doi: 10.1007/s11430-018-9190-x.

[11] Y.-L. Lee Chen, "Spatial and seasonal variations of nitrate-based new production and primary production in the South China Sea," *Deep Sea Res. I, Oceanographic Res. Papers*, vol. 52, no. 2, pp. 319–340, Feb. 2005.

[12] X. Chen, D. Pan, Y. Bai, X. He, and T. Wang, "Are the trends in the surface chlorophyll opposite between the South China Sea and the Bay of Bengal?" *Proc. SPIE*, vol. 9240, pp. 270–277, Oct. 2014, doi: 10.1117/12.2067584.

[13] M. J. Perry, "Assessing marine primary production from space," *BioScience*, vol. 36, no. 7, pp. 461–467, Aug. 1986.

[14] D. Antoine and A. Morel, "Oceanic primary production: 1. Adaptation of a spectral light-photosynthesis model in view of application to satellite chlorophyll observations," *Global Biogeochemical Cycles*, vol. 10, no. 1, pp. 43–55, Mar. 1996.

[15] K. R. Arrigo, G. L. van Dijken, and S. Bushinsky, "Primary production in the Southern Ocean, 1997–2006," *J. Geophys. Res.*, vol. 113, no. C8, pp. 1997–2006, 2008, doi: 10.1029/2007JC004551.

[16] M. J. Behrenfeld and P. G. Falkowski, "A consumer's guide to phytoplankton primary productivity models," *Limnology Oceanogr.*, vol. 42, no. 7, pp. 1479–1491, Nov. 1997.

[17] S. Sathyendranath, A. Longhurst, C. M. Caverhill, and T. Platt, "Regionally and seasonally differentiated primary production in the North Atlantic," *Deep Sea Res. I, Oceanographic Res. Papers*, vol. 42, no. 10, pp. 1773–1802, Oct. 1995.

[18] H. Zhao, D. Tang, and Y. Wang, "Comparison of phytoplankton Blooms triggered by two typhoons with different intensities and translation speeds in the South China Sea," *Mar. Ecol. Prog. Ser.*, vol. 365, pp. 57–65, Aug. 2008.

[19] T. Li et al., "Phytoplankton size classes changed oppositely over shelf and basin areas of the South China Sea during 2003–2018," *Prog. Oceanogr.*, vol. 191, Feb. 2021, Art no. 102496, doi: 10.1016/j.pocean.2020.102496.

[20] F. Kong, Q. Dong, K. Xiang, Z. Yin, Y. Li, and J. Liu, "Spatiotemporal variability of remote sensing ocean net primary production and major forcing factors in the tropical Eastern Indian and Western Pacific Ocean," *Remote Sens.*, vol. 11, no. 4, p. 391, Feb. 2019, doi: 10.3390/rs11040391.

[21] K. Zhou, M. Dai, K. Maiti, W. Chen, and Y. Xie, "Impact of physical and biogeochemical forcing on particle export in the South China Sea," *Prog. Oceanogr.*, vol. 187, Aug. 2020, Art. no. 102403.

[22] S.-C. Tan and G.-Y. Shi, "Spatiotemporal variability of satellite-derived primary production in the South China Sea, 1998–2006," *J. Geophys. Res.*, vol. 114, no. G3, pp. 1–11, Sep. 2009.

[23] X. Li, C. Chen, P. Shi, H. Zhan, and Q. He, "Estimation of primary production of South China Sea from 1998 to 2002 by remote sensing and its spatio–temporal variation mechanism," *J. Tropical Oceanogr.*, vol. 25, no. 3, pp. 57–62, 2006.

[24] J. Campbell et al., "Comparison of algorithms for estimating ocean primary production from surface chlorophyll, temperature, and irradiance," *Global Biogeochemical cycles*, vol. 16, no. 3, pp. 1–15, 2002, doi: 10.1029/2001GB001444.

[25] M. Carr et al., "A comparison of global estimates of marine primary production from ocean color," *Deep Sea Res. II, Top. Studies Oceanography*, vol. 53, pp. 741–770, Mar. 2006.

[26] S. Milutinović and L. Bertino, "Assessment and propagation of uncertainties in input terms through an ocean-color-based model of primary productivity," *Remote Sens. Environ.*, vol. 115, no. 8, pp. 1906–1917, Aug. 2011.

[27] Z. Lee and J. F. Marra, "The use of VGPM to estimate oceanic primary production: A 'Tango' difficult to dance," *J. Remote Sens.*, vol. 2022, Jan. 2022, Art. no. 9851013, doi: 10.34133/2022/9851013.

[28] M. J. Behrenfeld, E. Boss, D. A. Siegel, and D. M. Shea, "Carbon-based ocean productivity and phytoplankton physiology from space," *Global Biogeochem. Cycles*, vol. 19, no. 1, Mar. 2005, Art. no. GB1006, doi: 10.1029/2004GB002299.

[29] T. Westberry, M. J. Behrenfeld, D. A. Siegel, and E. Boss, "Carbon-based primary productivity modeling with vertically resolved photoacclimation," *Global Biogeochem. Cycles*, vol. 22, no. 2, pp. 1–18, Jun. 2008, doi: 10.1029/2007GB003078.

[30] Z. Lee, J. Marra, M. J. Perry, and M. Kahru, "Estimating oceanic primary productivity from ocean color remote sensing: A strategic assessment," *J. Mar. Syst.*, vol. 149, pp. 50–59, Sep. 2015.

[31] Z. P. Lee, K. L. Carder, J. Marra, R. G. Steward, and M. J. Perry, "Estimating primary production at depth from remote sensing," *Appl. Opt.*, vol. 35, pp. 463–474, Jan. 1996.

[32] T. Hirawake, S. Takao, N. Horimoto, T. Ishimaru, Y. Yamaguchi, and M. Fukuchi, "A phytoplankton absorption-based primary productivity model for remote sensing in the Southern Ocean," *Polar Biol.*, vol. 34, no. 2, pp. 291–302, Feb. 2011.

[33] Z. Lee et al., "An assessment of optical properties and primary production derived from remote sensing in the Southern Ocean (SO GasEx)," *J. Geophys. Res.*, vol. 116, Apr. 2011, Art. no. C00F03, doi: 10.1029/2010JC006747.

[34] A. Morel, "Optical modeling of the upper ocean in relation to its biogenous matter content (case I waters)," *J. Geophys. Res., Oceans*, vol. 93, no. C9, pp. 10749–10768, 1988.

[35] D. A. Kiefer and B. G. Mitchell, "A simple, steady state description of phytoplankton growth based on absorption cross section and quantum efficiency," *Limnology Oceanogr.*, vol. 28, no. 4, pp. 770–776, Jul. 1983.

[36] A. Morel, D. Antoine, M. Babin, and Y. Dandonneau, "Measured and modeled primary production in the northeast Atlantic (EUMELI JGOFS program): The impact of natural variations in photosynthetic parameters on model predictive skill," *Deep Sea Res. I, Oceanographic Res. Papers*, vol. 43, no. 8, pp. 1273–1304, Aug. 1996.

[37] T. Platt, C. L. Gallegos, and W. G. Harrison, "Photoinhibition of photosynthesis in natural assemblages of marine phytoplankton," *J. Mar. Res.*, vol. 38, no. 4, pp. 687–701, Jan. 1980.

[38] M. L. Zoffoli, Z. Lee, and J. F. Marra, "Regionalization and dynamic parameterization of quantum yield of photosynthesis to improve the ocean primary production estimates from remote sensing," *Frontiers Mar. Sci.*, vol. 5, p. 446, Nov. 2018.

[39] E. S. Nielsen, "The use of radio-active carbon (C^{14}) for measuring organic production in the sea," *ICES J. Mar. Sci.*, vol. 18, no. 2, pp. 117–140, Aug. 1952.

[40] Z.-P. Lee, Y.-H. Ahn, C. Mobley, and R. Arnone, "Removal of surface-reflected light for the measurement of remote-sensing reflectance from an above-surface platform," *Opt. Exp.*, vol. 18, no. 25, pp. 26313–26342, 2010.

[41] S. Tassan, "A sensitivity analysis of the 'transmittance-reflectance' method for measuring light absorption by aquatic particles," *J. Plankton Res.*, vol. 24, no. 8, pp. 757–774, Aug. 2002.

[42] Q. Dong, H. Hong, and S. Shang, "A new approach to correct for path-length amplification in measurements of particulate spectral absorption by the quantitative filter technique," *J. Xiamen Univ.*, vol. 47, no. 4, pp. 556–561, Jul. 2008.

[43] Q. Dong, S. Shang, and Z. Lee, "An algorithm to retrieve absorption coefficient of chromophoric dissolved organic matter from ocean color," *Remote Sens. Environ.*, vol. 128, pp. 259–267, Jan. 2013.

[44] B. Huang, J. Hu, H. Xu, Z. Cao, and D. Wang, "Phytoplankton community at warm eddies in the northern South China Sea in winter 2003/2004," *Deep Sea Res. II, Topical Stud. Oceanogr.*, vol. 57, nos. 19–20, pp. 1792–1798, Oct. 2010.

[45] Y. Xie, L. Lin, W. Xiao, X. Yu, W. Lan, and B. Huang, "Striking seasonal pattern of primary production in the river-dominated ocean margin of the northern South China Sea (NSCS-RiOMar) revealed by new field and remotely sensed data," *Prog. Oceanogr.*, vol. 189, Nov. 2020, Art. no. 102470, doi: 10.1016/j.pocean.2020.102470.

[46] W. Li et al., "Synergistic use of remote sensing and modeling for estimating net primary productivity in the red sea with VGPM, Eppley-VGPM, and CbPM models intercomparison," *IEEE Trans. Geosci. Remote Sens.*, vol. 58, no. 12, pp. 8717–8734, May 2020.

[47] T. Wang, P. Yu, Z. Wu, W. Lu, and B. Huang, "Revisiting the intraseasonal variability of chlorophyll—A in the adjacent luzon strait with a new gap-filled remote sensing data set," *IEEE Trans. Geosci. Remote Sens.*, vol. 60, pp. 1–11, 2021.

[48] W. W. Gregg and C. S. Rousseaux, "Global ocean primary production trends in the modern ocean color satellite record (1998–2015)," *Environ. Res. Lett.*, vol. 14, no. 12, Dec. 2019, Art. no. 124011, doi: 10.1088/1748-9326/ab4667.

[49] *Remote Sensing of Ocean Colour in Coastal, and Other Optically-Complex, Waters*, S. Sathyendranath, Ed., Int. Ocean-Colour Coordinating Group, Dartmouth, NH, Canada, 2000.

[50] S. W. Bailey and P. J. Werdell, "A multi-sensor approach for the on-orbit validation of ocean color satellite data products," *Remote Sens. Environ.*, vol. 102, nos. 1–2, pp. 12–23, May 2006, doi: 10.1016/j.rse.2006.01.015.2006.

[51] M. A. M. Friedrichs et al., "Assessing the uncertainties of model estimates of primary productivity in the tropical Pacific Ocean," *J. Mar. Syst.*, vol. 76, pp. 113–133, Feb. 2009.

[52] G. M. Silsbe, M. J. Behrenfeld, K. H. Halsey, A. J. Milligan, and T. K. Westberry, "The CAFE model: A net production model for global ocean phytoplankton," *Global Biogeochem. Cycles*, vol. 30, no. 12, pp. 1756–1777, Dec. 2016, doi: 10.1002/2016gb005521.

[53] J. P. Siemer et al., "Recent trends in SST, Chl—A, productivity and wind stress in upwelling and open ocean areas in the upper Eastern north Atlantic subtropical gyre," *J. Geophys. Res.*, vol. 126, no. 8, Aug. 2021, Art. no. e2021JC017268, doi: 10.1029/2021jc017268.

[54] C. Deser, M. A. Alexander, S.-P. Xie, and A. S. Phillips, "Sea surface temperature variability: Patterns and mechanisms," *Annu. Rev. Mar. Sci.*, vol. 2, no. 1, pp. 115–143, Jan. 2010, doi: 10.1146/annurev-marine-120408-151453.

[55] P. Xiu and F. Chai, "Variability of oceanic carbon cycle in the north Pacific from seasonal to decadal scales," *J. Geophys. Res., Oceans*, vol. 119, no. 8, pp. 5270–5288, Aug. 2014, doi: 10.1002/2013jc009505.

[56] J. Ma, H. Zhan, and Y. Du, "Seasonal and interannual variability of surface CDOM in the South China Sea associated with El Niño," *J. Mar. Syst.*, vol. 85, nos. 3–4, pp. 86–95, Apr. 2011, doi: 10.1016/j.jmarsys.2010.12.006.

[57] L. Deng, W. Zhou, W. Cao, G. Wang, and S. Hu, "Evaluating semi-analytical algorithms for estimating inherent optical properties in the South China Sea," *Opt. Exp.*, vol. 28, no. 9, pp. 13155–13176, 2020.

[58] S. L. Shang, Q. Dong, C. M. Hu, G. Lin, Y. H. Li, and S. P. Shang, "On the consistency of MODIS chlorophyll a products in the northern South China Sea," *Biogeosciences*, vol. 11, no. 2, pp. 269–280, 2014, doi: 10.5194/bg-11-269-2014.

[59] S. Shang, Q. Dong, Z. Lee, Y. Li, Y. Xie, and M. Behrenfeld, "MODIS observed phytoplankton dynamics in the Taiwan strait: An absorption-based analysis," *Biogeosciences*, vol. 8, no. 4, pp. 841–850, Apr. 2011, doi: 10.5194/bg-8-841-2011.

[60] Y.-Y. Shih et al., "Comparison of primary production using in situ and satellite-derived values at the SEATS station in the South China Sea," *Frontiers Mar. Sci.*, vol. 8, Oct. 2021, Art. no. 747763.

[61] S. Ma et al., "Estimation of marine primary productivity from satellite-derived phytoplankton absorption data," *IEEE J. Sel. Topics Appl. Earth Observ. Remote Sens.*, vol. 7, no. 7, pp. 3084–3092, Jul. 2014, doi: 10.1109/jstars.2014.2298863.

[62] J. Marra, C. Ho, and C. Trees, "An alternative algorithm for the calculation of primary productivity from remote sensing data," Lamont Doherty Earth Observatory Columbia Univ., New York, NY, USA, Tech. Rep., 2003.

[63] C.-C. Chen, F.-K. Shiah, S.-W. Chung, and K.-K. Liu, "Winter phytoplankton Blooms in the shallow mixed layer of the South China Sea enhanced by upwelling," *J. Mar. Syst.*, vol. 59, nos. 1–2, pp. 97–110, Jan. 2006.

[64] Y.-L. Lee Chen and H.-Y. Chen, "Seasonal dynamics of primary and new production in the northern South China Sea: The significance of river discharge and nutrient advection," *Deep Sea Res. I, Oceanographic Res. Papers*, vol. 53, no. 6, pp. 971–986, Jun. 2006, doi: 10.1016/j.dsr.2006.02.005.

[65] W. Lu, L.-Y. Oey, E. Liao, W. Zhuang, X.-H. Yan, and Y. Jiang, "Physical modulation to the biological productivity in the summer Vietnam upwelling system," *Ocean Sci.*, vol. 14, no. 5, pp. 1303–1320, Oct. 2018, doi: 10.5194/os-14-1303-2018.

[66] S. Shang, L. Li, J. Li, Y. Li, G. Lin, and J. Sun, "Phytoplankton Bloom during the northeast monsoon in the Luzon strait bordering the Kuroshio," *Remote Sens. Environ.*, vol. 124, pp. 38–48, Sep. 2012, doi: 10.1016/j.rse.2012.04.022.

[67] W. Lu, X.-H. Yan, and Y. Jiang, "Winter Bloom and associated upwelling northwest of the Luzon island: A coupled physical-biological modeling approach," *J. Geophys. Res., Oceans*, vol. 120, no. 1, pp. 533–546, Jan. 2015, doi: 10.1002/2014JC010218.

[68] G. Chen, P. Xiu, and F. Chai, "Physical and biological controls on the summer chlorophyll Bloom to the east of Vietnam," *J. Oceanogr.*, vol. 70, no. 3, pp. 323–328, Jun. 2014, doi: 10.1007/s10872-014-0232-x.

[69] J. F. Marra et al., "A database of ocean primary productivity from the C-14 method," *Limnol. Oceanogr. Lett.*, vol. 6, no. 2, pp. 107–111, Apr. 2021, doi: 10.1002/lol2.10175.

[70] A. Knap, A. Michaels, A. Close, H. Ducklow, and A. Dickson, "Protocols for the joint global ocean flux study (JGOFS) core measurements," Reprint IOC Manuals Guides, UNESCO, Paris, France, JGOFS Rep. 29, 1996.

[71] D. Antoine et al., "Assessment of uncertainty in the ocean reflectance determined by three satellite ocean color sensors (MERIS, SeaWiFS and MODIS-A) at an offshore site in the Mediterranean Sea (BOUSSOLE project)," *J. Geophys. Res.*, vol. 113, Jul. 2008, Art. no. C07013, doi: 10.1029/2007JC004472.

[72] B. B. Cael, "Variability-based constraint on ocean primary production models," *Limnology Oceanogr. Lett.*, vol. 6, no. 5, pp. 262–269, Oct. 2021, doi: 10.1002/lol2.10196.

[73] G. Zibordi, J. F. Berthon, F. Mélin, D. D'Alimonte, and S. Kaitala, "Validation of satellite ocean color primary products at optically complex coastal sites: Northern Adriatic Sea, Northern Baltic Proper and Gulf of Finland," *Remote Sens. Environ.*, vol. 113, no. 12, pp. 2574–2591, 2009.

[74] "Synergy between ocean colour and biogeochemical/ecosystem models," in *Proc. Reports Int. Ocean Colour Coordinating Group (IOCCG)*, no. 19, S. Dutkiewicz, Ed. Dartmouth, NS, Canada, 2020, pp. 1–184.

[75] J. Marra, C. C. Trees, and J. E. O'Reilly, "Phytoplankton pigment absorption: A strong predictor of primary productivity in the surface ocean," *Deep Sea Res. I, Oceanographic Res. Papers*, vol. 54, no. 2, pp. 155–163, Feb. 2007.

[76] *Remote Sensing of Inherent Optical Properties: Fundamentals, Tests of Algorithms, and Applications*, Rep. Int. Ocean-Colour Coordinating Group, vol. 5, Z.-P. Lee and V. Stuart, Ed., IOCCG, Dartmouth, NH, Canada, 2006, p. 126.

[77] T. J. Smyth, G. F. Moore, T. Hirata, and J. Aiken, "Semianalytical model for the derivation of ocean color inherent optical properties: Description, implementation, and performance assessment," *Appl. Opt.*, vol. 45, no. 31, pp. 8116–8131, 2006.

[78] Z. Lee and K. L. Carder, "Absorption spectrum of phytoplankton pigments derived from hyperspectral remote-sensing reflectance," *Remote Sens. Environ.*, vol. 89, no. 3, pp. 361–368, Feb. 2004.

[79] Z. P. Lee and K. L. R. C. Arnone, "Deriving inherent optical properties from water color: A multi-band quasi-analytical algorithm for optically deep waters," *Appl. Opt.*, vol. 41, pp. 5755–5772, Sep. 2002.

[80] P. J. Werdell et al., "Generalized ocean color inversion model for retrieving marine inherent optical properties," *Appl. Opt.*, vol. 52, no. 10, pp. 2019–2037, 2013.

[81] J. Marra, C. C. Trees, R. R. Bidigare, and R. T. Barber, "Pigment absorption and quantum yields in the Arabian Sea," *Deep Sea Res. II, Topical Stud. Oceanogr.*, vol. 47, nos. 7–8, pp. 1279–1299, Jan. 2000.

[82] M. Babin, "Nitrogen-and irradiance-dependent variations of the maximum quantum yield of carbon fixation in eutrophic, mesotrophic and oligotrophic marine systems," *Deep Sea Res. I, Oceanographic Res. Papers*, vol. 43, no. 8, pp. 1241–1272, 1996.

[83] D. Iluz and Z. Dubinsky, "Quantum yields in aquatic photosynthesis," in *Photosynthesis*, Z. Dubinsky, Ed. Israel: IntechOpen, 2013, pp. 135–158, doi: 10.5772/56539 .

[84] M. Ostrowska, B. Wozniak, and J. Dera, "Modelled quantum yields and energy efficiency of fluorescence, photosynthesis and heat production by phytoplankton in the world ocean," *Oceanologia*, vol. 54, no. 4, pp. 565–610, 2012, doi: 10.5697/oc.54-4.565.

[85] J. Wu et al., "Estimates of diurnal and daily net primary productivity using the geostationary ocean color imager (GOCI) data," *Remote Sens. Environ.*, vol. 280, Oct. 2022, Art. no. 113183, doi: 10.1016/j.rse.2022.113183.

[86] T. Platt, S. Sathyendranath, O. Ulloa, W. G. Harrison, N. Hoepffner, and J. Goes, "Nutrient control of phytoplankton photosynthesis in the western North Atlantic," *Nature*, vol. 356, no. 6366, pp. 229–231, Mar. 1992.

[87] R. R. Bidigare, M. E. Ondrusek, J. H. Morrow, and D. A. Kiefer, "In vivo absorption properties of algal pigments," *Proc. SPIE*, vol. 1302, pp. 290–302, Sep. 1990.

[88] A. Bricaud, A.-L. Bédhomme, and A. Morel, "Optical properties of diverse phytoplanktonic species: Experimental results and theoretical interpretation," *J. Plankton Res.*, vol. 10, no. 5, pp. 851–873, 1988.

[89] A. Bricaud, M. Babin, A. Morel, and H. Claustre, "Variability in the chlorophyll-specific absorption coefficients of natural phytoplankton: Analysis and parameterization," *J. Geophys. Res., Oceans*, vol. 100, no. C7, pp. 13321–13332, 1995.

[90] M. Bellacicco, J. Pitarch, E. Organelli, V. Martinez-Vicente, G. Volpe, and S. Marullo, "Improving the retrieval of carbon-based phytoplankton biomass from satellite ocean colour observations," *Remote Sens.*, vol. 12, no. 21, p. 3640, Nov. 2020.

[91] W. Xu, G. Wang, L. Jiang, X. Cheng, W. Zhou, and W. Cao, "Spatiotemporal variability of surface phytoplankton carbon and carbon-to-chlorophyll a ratio in the South China Sea based on satellite data," *Remote Sens.*, vol. 13, no. 1, p. 30, Dec. 2020.

[92] Z. Lee, R. Arnone, C. Hu, P. J. Werdell, and B. Lubac, "Uncertainties of optical parameters and their propagations in an analytical ocean color inversion algorithm," *Appl. Opt.*, vol. 49, no. 3, pp. 369–381, 2010.

[93] M. J. Behrenfeld and E. Boss, "The beam attenuation to chlorophyll ratio: An optical index of phytoplankton physiology in the surface ocean?" *Deep Sea Res. I, Oceanographic Res. Papers*, vol. 50, no. 12, pp. 1537–1549, Dec. 2003.

[94] M. J. Behrenfeld et al., "Revaluating ocean warming impacts on global phytoplankton," *Nature Climate Change*, vol. 6, no. 3, pp. 323–330, 2015.

[95] "Uncertainties in ocean colour remote sensing," in *Proc. Reports Int. Ocean Colour Coordinating Group (IOCCG)*, no. 18, F. Mélin, Ed. Dartmouth, NS, Canada, 2019, pp. 1–164.

[96] R. Frouin and R. T. Pinker, "Estimating photosynthetically active radiation (PAR) at the Earth's surface from satellite observations," *Remote Sens. Environ.*, vol. 51, no. 1, pp. 98–107, Jan. 1995.

[97] L. J. Cheng et al., "Record-setting ocean warmth continued in 2019," *Adv. Atmos. Sci.*, vol. 37, no. 2, pp. 137–142, Feb. 2020, doi: 10.1007/s00376-020-9283-7.

[98] G. C. Li, L. J. Cheng, J. Zhu, K. E. Trenberth, M. E. Mann, and J. P. Abraham, "Increasing ocean stratification over the past half-century," *Nature Climate Change*, vol. 10, no. 12, p. 1116, Dec. 2020, doi: 10.1038/s41558-020-00918-2.

[99] D. M. Karl et al., "Temporal studies of biogeochemical processes determined from ocean time-series observations during the JGOFS era," in *Ocean Biogeochemistry*, M. J. R. Fasham, Ed. Berlin, Germany: Springer, 2003, pp. 239–267.

[100] G. T. F. Wong, C.-M. Tseng, L.-S. Wen, and S.-W. Chung, "Nutrient dynamics and N-anomaly at the SEATS station," *Deep Sea Res. II, Topical Stud. Oceanogr.*, vol. 54, nos. 14–15, pp. 1528–1545, Jul. 2007.